Computation of the diffraction from complex illumination sources in extended regions of space

G. Karagounis,* D. De Zutter, and D. Vande Ginste

Department of Information Technology, Ghent University, 9000, Ghent, Belgium

**giorgos.karagounis@intec.ugent.be*

Abstract: In this paper, a two-dimensional high-frequency formalism is presented which describes the diffraction of arbitrary wavefronts incident on edges of an otherwise smooth surface. The diffracted field in all points of a predefined region of interest is expressed in terms of the generalized Huygens representation of the incident field and a limited set of translation coefficients that take into account the arbitrary nature of the incident wavefront and its diffraction. The method is based on the Uniform Theory of Diffraction (UTD) and can therefore be utilized for every canonical problem for which the UTD diffraction coefficient is known. Moreover, the proposed technique is easy to implement as only standard Fast Fourier Transform (FFT) routines are required. The technique's validity is confirmed both theoretically and numerically. It is shown that for fields emitted by a discrete line source and diffracted by a perfectly conducting wedge, the method is in excellent agreement with the analytic solution over the entire simulation domain, including regions near shadow and reflection boundaries. As an application example, the diffraction in the presence of a perfectly conducting wedge illuminated by a complex light source is analyzed, demonstrating the appositeness of the method.

OCIS codes: (260.1960) Diffraction theory; (260.2110) Electromagnetic optics.

References and links

1. G. Pelosi and S. Selleri, "The wedge-type problem: The building brick in high-frequency scattering from complex objects," IEEE Antennas Propag. Mag. **55**, 41–58 (2013).
2. J. B. Keller, "Geometrical theory of diffraction," J. Opt. Soc. Am. **52**, 116–130 (1961).
3. R. G. Kouyoumjian and P. H. Pathak, "A uniform geometrical theory of diffraction for an edge in a perfectly conducting surface," Proc. IEEE **62**, 1448–1461 (1974).
4. P. Pathak, W. Burnside, and R. J. Marhefka, "A uniform GTD analysis of the diffraction of electromagnetic waves by a smooth convex surface," IEEE Trans. Antennas Propag. **28**, 631–642 (1980).
5. Y. Rahmat-Samii and R. Mittra, "Spectral analysis of high-frequency diffraction of an arbitrary incident field by a half plane-comparison with four asymptotic techniques," Radio Sci. **13**, 31–48 (1978).
6. Y. Z. Umul, "Scattering of a line source by a cylindrical parabolic impedance surface," J. Opt. Soc. Am. A **25**, 1652–1659 (2008).
7. "NIST digital library of mathematical functions," http://dlmf.nist.gov/, Release 1.0.5 of 2012-10-01. Online companion to [12].
8. L. B. Felsen and N. Marcuvitz, *Radiation and Scattering of Waves* (IEEE Press, 1994).
9. Y. Z. Umul, "Scattering of a Gaussian beam by an impedance half-plane," J. Opt. Soc. Am. A **24**, 3159–3167 (2007).

10. A. C. Green, H. L. Bertoni, and L. B. Felsen, "Properties of the shadow cast by a half-screen when illuminated by a Gaussian beam," J. Opt. Soc. Am. **69**, 1503–1508 (1979).
11. G. Suedan and E. Jull, "Beam diffraction by half planes and wedges: Uniform and asymptotic solutions," J Electromagnet Wave **3**, 17–26 (1989).
12. F. W. J. Olver, D. W. Lozier, R. F. Boisvert, and C. W. Clark, *NIST Handbook of Mathematical Functions* (Cambridge University, 2010). Print companion to [7].

---

1. Introduction

During the last few decades, high-frequency methods have contributed substantially to the understanding of diffraction. Different formalisms established between 1970 and 1990 remain useful to this day [1]. On the one hand, the Geometrical Theory of Diffraction (GTD) [2] and the Uniform Theory of Diffraction (UTD) [3], which overcomes some shortcomings of GTD, are still used extensively due to the simplicity of their implementation. Despite the popularity of UTD, in essence, it can only be used to study the diffraction of plane waves or fields emitted by discrete sources. GTD is applicable to any kind of illumination, but it is less accurate than UTD close to the diffraction edge and it does not provide the correct solution over the entire space, as its solution is singular at transition regions. On the other hand, formalisms that can deal with complex source configurations [4, 5] often miss transparency and/or are very intricate and as such are less likely to be used in practice. Because of this, scattering by large objects is either studied using full-wave electromagnetic solvers, which require large amounts of memory and computing time, or the original problem is simplified so that the high-frequency methods can still be used, leading to loss of accuracy.

The high-frequency formalism that is presented in this paper describes the diffraction of arbitrary incident fields. As the formalism is based on UTD, it can be used for every geometry for which the UTD diffraction coefficient is available. In addition, the field over an extended region of space is obtained using the generalized Huygens representation of the incident field and a limited set of translation coefficients. The technique has been presented in a transparent way and can readily be used in applications, this in contrast to the Spectral Theory of Diffraction (STD) [5].

In Sec. 2, we present the new formalism preceded by a short review of UTD. The validity of the new formalism is established both theoretically and experimentally in Sec. 3. A realistic application example is treated in Sec. 4. Conclusions are formulated in Sec. 5.

2. Formalism

To clearly explain and illustrate the technique, in this paper, we deal with two-dimensional transverse magnetic (TM) problems. An $\exp(j\omega t)$ time dependence, with ω being the angular frequency, is assumed and supressed throughout the text.

2.1. *Uniform theory of diffraction*

In the original paper of Kouyoumjian and Pathak [3], a high-frequency solution for the diffraction of an electromagnetic wave at an edge in an otherwise smooth surface is presented. The total field is represented as a sum of three contributions arising from the ray-optical field. The *direct contribution* is related to the field of the source in the absence of the surface. The *reflection contribution* describes the field reflected from the surface if the diffracting edge is ignored and the *diffraction contribution* describes the edge-diffracted field. The main advantage of UTD compared to previous approaches [2] is that its solution remains valid in the *transition regions*, where the separate ray-optical contributions may vary rapidly, although the total field remains smooth. In the neighbourhood of the *shadow boundary* (SB) the direct and the diffraction contributions vary rapidly, while at the *reflection boundary* (RB) the reflection and the diffraction

#199158 - $15.00 USD Received 8 Oct 2013; revised 18 Nov 2013; accepted 19 Nov 2013; published 3 Dec 2013

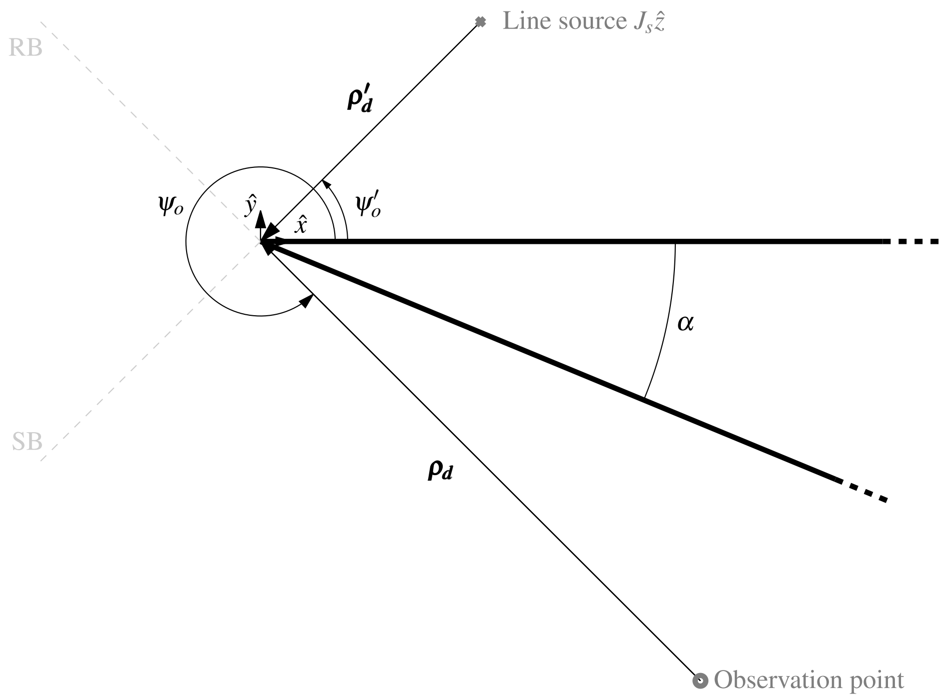

Fig. 1. Canonical problem geometry. A single line source illuminates the wedge, leading to a (diffracted) field at a single, discrete observation point. The shadow boundary and the reflection boundary are also indicated.

contributions vary quickly. A diffraction coefficient is introduced to describe the contribution due to diffraction of the incident field on the edge. The coefficient depends on a distance parameter L which itself also depends on the type of illumination. It is important to mention that this dependence limits the use of UTD to incident fields for which L is known, in contrast to the novel technique presented in Sec. 2.2 that deals with arbitrary sources and incident fields.

In [3] special attention is given to the canonical case of diffraction by a straight, perfectly conducting wedge of opening angle α residing in free space. The geometry is shown in Fig. 1. The tip of the wedge resides at the origin of the coordinate system $(\hat{x},\hat{y})$. The vector pointing from the current line source to the edge is denoted by $\boldsymbol{\rho_d'}$. The source resides at an angle ψ_o' measured from the $\hat{x}$-axis. For the observation point, the same notation is used apart from omitting the prime $'$. For a current J_s flowing in the positive $\hat{z}$-direction, the contribution due to diffraction is given by

$$E_z^{diff}(-\boldsymbol{\rho_d}) = -J_s\frac{\omega\mu_0}{4}H_0^{(2)}(k\rho_d')D_{UTD}(L;\boldsymbol{\rho_d'},-\boldsymbol{\rho_d})\frac{e^{-jk\rho_d}}{\sqrt{\rho_d}}, \tag{1}$$

where μ_0 is the permeability of free space, k is the wavenumber, $H_0^{(2)}$ stands for the Hankel function of the second kind and of zeroth order, $\rho_d' = |\ \boldsymbol{\rho_d'}\ |$ and $\rho_d = |\ \boldsymbol{\rho_d}\ |$. The diffraction coefficient $D_{UTD}(L;\boldsymbol{\rho_d'},-\boldsymbol{\rho_d})$ is [3]

#199158 - $15.00 USD Received 8 Oct 2013; revised 18 Nov 2013; accepted 19 Nov 2013; published 3 Dec 2013

$$
\begin{aligned}
D_{UTD}(L;\boldsymbol{\rho_d'},-\boldsymbol{\rho_d}) \quad = \quad & -\frac{1-j}{4(2\pi-\alpha)}\sqrt{\frac{\pi}{k}}\left[\cot\left(\frac{\pi(\pi+\psi_o-\psi_o')}{2(2\pi-\alpha)}\right)F\left(kLa^{+}(\psi_o-\psi_o')\right)\right.\\
&+\cot\left(\frac{\pi(\pi-\psi_o+\psi_o')}{2(2\pi-\alpha)}\right)F\left(kLa^{-}(\psi_o-\psi_o')\right)\\
&-\cot\left(\frac{\pi(\pi+\psi_o+\psi_o')}{2(2\pi-\alpha)}\right)F\left(kLa^{+}(\psi_o+\psi_o')\right)\\
&\left.-\cot\left(\frac{\pi(\pi-\psi_o-\psi_o')}{2(2\pi-\alpha)}\right)F\left(kLa^{-}(\psi_o+\psi_o')\right)\right],
\end{aligned}
\tag{2}
$$

where

$$
F(X)=2j\sqrt{X}e^{jX}\int_{\sqrt{X}}^{+\infty}\mathrm{d}\tau\, e^{-j\tau^2} \tag{3}
$$

is related to the Fresnel functions. Furthermore, the functions a^{+} and a^{-} in Eq. (2) are defined as

$$
a^{\pm}(\beta)=2\cos^2\left(\frac{2(2\pi-\alpha)N^{\pm}-\beta}{2}\right), \tag{4}
$$

with β the argument of the functions and where $N^{\pm}$ are integers that most closely satisfy

$$
2(2\pi-\alpha)N^{\pm}-\beta=\pm\pi. \tag{5}
$$

For this specific case of cylindrical-wave incidence, the distance parameter L is given by

$$
L=\frac{\rho_d\rho_d'}{\rho_d+\rho_d'}, \tag{6}
$$

which is a well-established result (see e.g. [3]). Note that in e.g. [6] canonical UTD diffraction coefficients are derived for more intricate problem geometries. The method presented in the next section is also applicable in these cases.

2.2. *Improved UTD-based technique*

In this section, the new formalism is derived. It will be shown that by leveraging standard FFT routines, the diffracted field for an arbitrary, spatially distributed source configuration is readily computed. The derivation consists of two phases. First, a Huygens representation is derived for the arbitrary incident field. This enables to write down a UTD type representation of the scattered fields. Second, an angular harmonics expansion of the field within a particular region of interest is introduced in which translation coefficients connect the angular harmonics of the incident and the diffracted fields.

The geometry of the problem is illustrated in Fig. 2. Diffraction by a straight, perfectly conducting wedge is considered again, although the formalism is applicable to any canonical problem for which the diffraction coefficient is known. The tip of the wedge resides once more at the origin of the coordinate system $(\hat{x},\hat{y})$. The distributed source is indicated in light gray hatching in the figure. A local cartesian coordinate system $(\hat{\xi}',\hat{\eta}')$ is attached to this source configuration, from which the local polar coordinates (ρ',ϕ') are derived. With respect to the $(\hat{\xi}',\hat{\eta}')$ system, the wedge resides at $\boldsymbol{\rho_d'}$, making an angle ϕ_o' measured from the $\hat{\xi}'$-axis. Conversely, the origin of this local coordinate system resides at an angle ψ_o' measured from the $\hat{x}$-axis. The

#199158 - $15.00 USD Received 8 Oct 2013; revised 18 Nov 2013; accepted 19 Nov 2013; published 3 Dec 2013

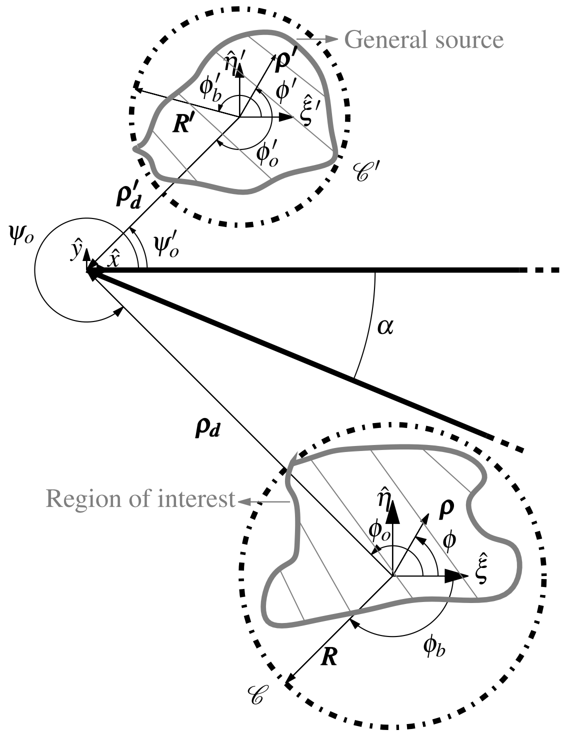

Fig. 2. Canonical problem geometry. An arbitrary, spatially distributed light source (hatched light gray) illuminates the wedge, leading to a (diffracted) field within a user-defined, spatially distributed region of interest (hatched light gray).

distributed source is circumscribed by a circle $\mathscr{C}'$ with radius R' centered about the origin of the local coordinate system (dash-dot line in the figure). This circle is described by position vector $\boldsymbol{R'}$, making an angle ϕ'_b measured from the $\hat{\xi}'$-axis. Similarly, the region of interest is also indicated on the figure, a local coordinate system is attached to it and its circumscribing circle $\mathscr{C}$ is drawn. Apart from omitting the prime $'$, the same notation as for the source region is used. The question that now arises is how to efficiently compute the field within the complete region of interest.

In the first phase, we derive a Huygens representation for the distributed source configuration. This is possible by the identification of the angular harmonics expansion of the incoming field with the field emitted by the equivalent Huygens sources on the boundary $\mathscr{C}'$. So, on the one hand, the $\hat{z}$-oriented electric field for a given TM-polarized source is easily decomposed into cylindrical harmonics in the $(\hat{\xi}', \hat{\eta}')$ coordinate system:

$$E_z^{inc}(\boldsymbol{\rho'}) = -\frac{\omega\mu_0}{4} \sum_{q'=-\infty}^{\infty} a_{q'} H_{q'}^{(2)}(k\rho') e^{jq'\phi'}, \quad \rho' > R', \tag{7}$$

where $H_{q'}^{(2)}$ stands for the Hankel function of the second kind and of order q', $\rho' = |\, \boldsymbol{\rho'} \,|$ and $R' = |\, \boldsymbol{R'} \,|$. The coefficients $a_{q'}$ are related to the incident field on the boundary $\mathscr{C}'$ as follows:

$$a_{q'} = -\frac{2}{\pi\omega\mu_0 H_{q'}^{(2)}(kR')} \int_{-\pi}^{\pi} \mathrm{d}\phi'_b \, E_z^{inc}(\boldsymbol{R'}) e^{-jq'\phi'_b}. \tag{8}$$

#199158 - $15.00 USD Received 8 Oct 2013; revised 18 Nov 2013; accepted 19 Nov 2013; published 3 Dec 2013

Hence, upon knowledge of $E_z^{inc}(\boldsymbol{R'})$, they can be efficiently computed by means of a FFT.

On the other hand, by virtue of Huygens' principle, $\hat{z}$-oriented current sources $\mathscr{J}_z(\boldsymbol{R'})$ on $\mathscr{C}'$ that produce the same field as in Eq. (7) for $\rho' > R'$ are now identified. Thereto, consider the field radiated by these equivalent sources:

$$E_z^{inc}(\boldsymbol{\rho'}) = -\frac{\omega\mu_0}{4}\int_{-\pi}^{\pi} R' \mathrm{d}\phi_b' \, \mathscr{J}_z(\boldsymbol{R'}) H_0^{(2)}(k \mid \boldsymbol{\rho'} - \boldsymbol{R'} \mid). \tag{9}$$

Given the periodicity along $\mathscr{C}'$, $\mathscr{J}_z(\boldsymbol{R'})$ is decomposed into its Fourier series

$$\mathscr{J}_z(\boldsymbol{R'}) = \sum_{q'=-\infty}^{\infty} I_{q'} e^{jq'\phi_b'}, \tag{10}$$

with as yet unknown coefficients $I_{q'}$. Graf's addition theorem [7] dictates that

$$H_0^{(2)}\left(k \mid \boldsymbol{\rho'} - \boldsymbol{R'} \mid\right) = \sum_{m=-\infty}^{\infty} H_m^{(2)}(k\rho') J_m(kR') e^{jm(\phi'-\phi_b')}, \quad \rho' > R', \tag{11}$$

Introducing Eq. (10) and Eq. (11) into Eq. (9) and identification with Eq. (7) yields

$$I_{q'} = \frac{a_{q'}}{2\pi R' J_{q'}(kR')}. \tag{12}$$

Finally, Eq. (9) is rewritten as:

$$E_z^{inc}(\boldsymbol{\rho'}) = -\frac{\omega\mu_0}{4}\sum_{q'=-\infty}^{\infty}\frac{a_{q'}}{2\pi J_{q'}(kR')}\int_{-\pi}^{\pi}\mathrm{d}\phi_b' H_0^{(2)}(k \mid \boldsymbol{\rho'} - \boldsymbol{R'} \mid) e^{jq'\phi_b'}, \tag{13}$$

which is the Huygens representation of the incident field. Through Eq. (8), the reader notices that $E_z^{inc}(\boldsymbol{\rho'})$ is expressed in terms of the incoming field on the circle $\mathscr{C}'$. Casting the known field radiated by the arbitrary source in the form of Eq. (13) is a crucial step. Indeed, Eq. (13) represents the field excited by the equivalent Huygens' line sources and hence, UTD as in Sec. 2.1 can be directly applied. By means of superposition, the diffracted field in $\boldsymbol{\rho}$, in the $(\hat{\xi}, \hat{\eta})$ coordinate system, is given by

$$\begin{aligned} E_z^{diff}(\boldsymbol{\rho}) = -\frac{\omega\mu_0}{4}\frac{e^{-jk|-\boldsymbol{\rho_d}+\boldsymbol{\rho}|}}{\sqrt{\mid -\boldsymbol{\rho_d}+\boldsymbol{\rho} \mid}}&\sum_{q'=-\infty}^{\infty}\frac{a_{q'}}{2\pi J_{q'}(kR')} \\ &\times\int_{-\pi}^{\pi}\mathrm{d}\phi_b' D_{UTD}\left(L;\boldsymbol{\rho_d'}-\boldsymbol{R'},-\boldsymbol{\rho_d}+\boldsymbol{\rho}\right) e^{jq'\phi_b'} H_0^{(2)}\left(k \mid \boldsymbol{\rho_d'}-\boldsymbol{R'} \mid\right). \end{aligned} \tag{14}$$

So, Eq. (14) already yields the diffracted field caused by a distributed source.

In the second phase, we derive an efficient way to describe the diffracted field in a predefined region of interest. To this end we expand the diffracted field in angular harmonics within the region of interest. The decomposition is similar to Eq. (7), i.e.

$$E_z^{diff}(\boldsymbol{\rho}) = -\frac{\omega\mu_0}{4}\sum_{q=-\infty}^{\infty} b_q J_q(k\rho) e^{jq\phi}, \tag{15}$$

with $\rho = \mid \boldsymbol{\rho} \mid < R$ and with the coefficients b_q given by

#199158 - $15.00 USD Received 8 Oct 2013; revised 18 Nov 2013; accepted 19 Nov 2013; published 3 Dec 2013

$$b_q = \frac{1}{2\pi J_q(kR)} \sum_{q'=-\infty}^{\infty} \frac{a_{q'}}{2\pi J_{q'}(kR')} \int_{-\pi}^{\pi} \mathrm{d}\phi_b \, \frac{e^{-jk|-\boldsymbol{\rho_d}+\boldsymbol{R}|}}{\sqrt{|-\boldsymbol{\rho_d}+\boldsymbol{R}|}} \times \int_{-\pi}^{\pi} \mathrm{d}\phi_b' D_{UTD}\left(L;\boldsymbol{\rho_d'}-\boldsymbol{R'},-\boldsymbol{\rho_d}+\boldsymbol{R}\right) e^{jq'\phi_b'} H_0^{(2)}\left(k\,|\,\boldsymbol{\rho_d'}-\boldsymbol{R'}\,|\right). \quad (16)$$

As the proposed formalism is valid at high frequencies, the high-frequency approximation of the 2-D Green's function, i.e. the Hankel function, is used to symmetrize Eq. (16) in the integrals over ϕ_b' and ϕ_b. This high-frequency approximation is given by [7]

$$H_0^{(2)}(k\,|-\boldsymbol{\rho_d}+\boldsymbol{R}\,|) \approx (1+j)\frac{e^{-jk|-\boldsymbol{\rho_d}+\boldsymbol{R}|}}{\sqrt{\pi k\,|-\boldsymbol{\rho_d}+\boldsymbol{R}\,|}}, \quad k\,|-\boldsymbol{\rho_d}+\boldsymbol{R}\,| \gg 1, \quad (17)$$

and substitution into Eq. (16) leads to

$$b_q \approx \frac{1}{2\pi J_q(kR)} \sum_{q'=-\infty}^{\infty} \frac{a_{q'}}{2\pi J_{q'}(kR')} \frac{1-j}{2}\sqrt{\pi k} \int_{-\pi}^{\pi} \mathrm{d}\phi_b \, H_0^{(2)}\left(k\,|-\boldsymbol{\rho_d}+\boldsymbol{R}\,|\right) \times \int_{-\pi}^{\pi} \mathrm{d}\phi_b' D_{UTD}\left(L;\boldsymbol{\rho_d'}-\boldsymbol{R'},-\boldsymbol{\rho_d}+\boldsymbol{R}\right) e^{jq'\phi_b'} H_0^{(2)}\left(k\,|\,\boldsymbol{\rho_d'}-\boldsymbol{R'}\,|\right). \quad (18)$$

Although Eq. (15) and Eq. (18) suffice to determine the diffracted field in the entire region of interest, the computation would be rather cumbersome as the integrand of the double integral is highly oscillatory with multiple, possibly coinciding, stationary points. Fortunately, this integration can be circumvented by again invoking Graf's addition theorem of Eq. (11), but now for $H_0^{(2)}(k\,|\,\boldsymbol{\rho_d'}-\boldsymbol{R'}\,|)$ and $H_0^{(2)}(|-\boldsymbol{\rho_d}+\boldsymbol{R}\,|)$. After some straightforward mathematical manipulations, the following final expression for the diffracted field is obtained:

$$E_z^{diff}(\boldsymbol{\rho}) \approx -\frac{\omega\mu_0}{4} \sum_{q=-\infty}^{\infty} \sum_{q'=-\infty}^{\infty} \frac{J_q(k\rho)e^{jq\phi}}{J_q(kR)} T_{q,q'} \frac{a_{q'}}{J_{q'}(kR')}, \quad (19)$$

with known coefficients $a_{q'}$ from Eq. (8) and translation coefficients

$$T_{q,q'} = \sum_{n=-\infty}^{\infty} H_n^{(2)}(k\rho_d) J_n(kR) e^{-jn\phi_o} \sum_{m=-\infty}^{\infty} \frac{1-j}{2}\sqrt{\pi k}\, d_{-n+q,m-q'} H_m^{(2)}(k\rho_d') J_m(kR') e^{jm\phi_o'}. \quad (20)$$

The translation coefficients $T_{q,q'}$ connect the angular harmonics expansion of the incident field to the expansion of the field within the region of interest. The coefficients $d_{-n+q,m-q'}$ in Eq. (20) are given by

$$d_{s,l} = \frac{1}{4\pi^2} \int_{-\pi}^{\pi} \mathrm{d}\phi_b \, e^{-js\phi_b} \int_{-\pi}^{\pi} \mathrm{d}\phi_b' \, e^{-jl\phi_b'} D_{UTD}\left(L;\boldsymbol{\rho_d'}-\boldsymbol{R'},-\boldsymbol{\rho_d}+\boldsymbol{R}\right), \quad (21)$$

and hence, they are efficiently computed via 2-D FFTs of the pertinent diffraction coefficient. Note indeed that the integrand in the 2-D FFT of Eq. (21) is no longer oscillatory.

In Sec. 3, it will be shown that retaining a limited number of terms in the infinite series of Eq. (19) and Eq. (20) leads to a good accuracy. In order not to overload the paper, however, we opt not to present a full convergence analysis, but restrict ourselves to providing the necessary insight to the reader. Given the large values of $k\rho' > kR'$ and small values $k\rho < kR$ in Eq. (7) and Eq. (15) respectively, these series converge rapidly. The series in Eq. (20) can also be truncated, retaining a limited number of terms, provided that only a limited set of coefficients $d_{s,l}$ contributes to this series. This is the case for a smooth, well-behaved integrand in the 2-D FFT computation in Eq. (21) and hence, at this point, it should be noted that the diffraction coefficient in the UTD theory is discontinuous at the transition regions. As a result, an accurate description of the diffracted field in regions of interest that cross the transition regions of the source configuration may not be guaranteed because of the Gibbs phenomenon. In order to avoid inaccuracies at transition regions for this kind of problems, rather than focusing on the diffracted field, we propose to describe the *total* field in a "UTD-like manner". Thereto, the total field at $\boldsymbol{\rho}$ in the $(\hat{\xi},\hat{\eta})$ system, due to a line source with unit current density in the $+\hat{z}$ direction at $\boldsymbol{\rho'}$ in the $(\hat{\xi}',\hat{\eta}')$ system, is written in the following way

$$\begin{aligned}
E_z^{tot}(\boldsymbol{\rho};\boldsymbol{\rho'}) &= E^{diff}(\boldsymbol{\rho};\boldsymbol{\rho'})+E^{refl}(\boldsymbol{\rho};\boldsymbol{\rho'})+E^{direct}(\boldsymbol{\rho};\boldsymbol{\rho'})\\
&\approx -\frac{\omega\mu_0}{4}H_0^{(2)}\left(k\,|\,\boldsymbol{\rho_d'}-\boldsymbol{\rho'}\,|\right)D_{UTD}\left(L;\boldsymbol{\rho_d'}-\boldsymbol{\rho'},-\boldsymbol{\rho_d}+\boldsymbol{\rho}\right)\\
&\quad\times\frac{1-j}{2}\sqrt{\pi k}H_0^{(2)}\left(k\,|-\boldsymbol{\rho_d}+\boldsymbol{\rho}\,|\right)+\frac{\omega\mu_0}{4}H_0^{(2)}\left(k\,|\,\boldsymbol{\rho_d''}-\boldsymbol{\rho''}-\boldsymbol{\rho_d}+\boldsymbol{\rho}\,|\right)u^{refl}\\
&\quad-\frac{\omega\mu_0}{4}H_0^{(2)}\left(k\,|\,\boldsymbol{\rho_d'}-\boldsymbol{\rho'}-\boldsymbol{\rho_d}+\boldsymbol{\rho}\,|\right)u^{direct}\\
&\equiv -\frac{\omega\mu_0}{4}H_0^{(2)}\left(k\,|\,\boldsymbol{\rho_d'}-\boldsymbol{\rho'}\,|\right)D'\left(L;\boldsymbol{\rho_d'}-\boldsymbol{\rho'},-\boldsymbol{\rho_d}+\boldsymbol{\rho}\right)\\
&\quad\times\frac{1-j}{2}\sqrt{\pi k}H_0^{(2)}\left(k\,|-\boldsymbol{\rho_d}+\boldsymbol{\rho}\,|\right).
\end{aligned}\tag{22}$$

The reflection and the direct contributions may both be different from zero depending on the position of the observer relative to the position of the source. Step functions u^{refl} and u^{direct} are added to the above expression to account for this. Vectors with superscript $''$ have a similar meaning as vectors with superscript $'$, but are related to image sources corresponding to reflection contributions. In the last step, a new coefficient $D'\left(L;\boldsymbol{\rho_d'}-\boldsymbol{\rho'},-\boldsymbol{\rho_d}+\boldsymbol{\rho}\right)$ is introduced, which equals

$$\begin{aligned}
D'\left(L;\boldsymbol{\rho_d'}-\boldsymbol{\rho'},-\boldsymbol{\rho_d}+\boldsymbol{\rho}\right) &= D_{UTD}\left(L;\boldsymbol{\rho_d'}-\boldsymbol{\rho'},-\boldsymbol{\rho_d}+\boldsymbol{\rho}\right)\\
&\quad+\frac{1+j}{\sqrt{\pi k}}\frac{1}{H_0^{(2)}\left(k\,|\,\boldsymbol{\rho_d'}-\boldsymbol{\rho'}\,|\right)H_0^{(2)}\left(k\,|-\boldsymbol{\rho_d}+\boldsymbol{\rho}\,|\right)}\times\\
&\left[-H_0^{(2)}\left(k\,|\,\boldsymbol{\rho_d''}-\boldsymbol{\rho''}-\boldsymbol{\rho_d}+\boldsymbol{\rho}\,|\right)u^{refl}+H_0^{(2)}\left(k\,|\,\boldsymbol{\rho_d'}-\boldsymbol{\rho'}-\boldsymbol{\rho_d}+\boldsymbol{\rho}\,|\right)u^{direct}\right].
\end{aligned}\tag{23}$$

The coefficient $D'\left(L;\boldsymbol{\rho_d'}-\boldsymbol{\rho'},-\boldsymbol{\rho_d}+\boldsymbol{\rho}\right)$ is continuous over the transition regions. Using D' instead of D_{UTD} in the formalism, and hence in Eq. (21), always ensures good accuracy over the transition regions. Additionally, by this substitution, one immediately obtains the sought for total field in the entire region of interest rather than the diffracted field.

3. Validation

3.1. Limit for infinitesimally small sources and regions of interest

When $\rho_d \gg R$ and $\rho_d' \gg R'$, i.e. when the dimensions of the source and the region of interest become negligible, the proposed formalism of Sec. 2.2 should reduce to the UTD formalism of Sec. 2.1. Indeed, with these assumptions we can write the Taylor series of the diffraction coefficient, only retaining the following dominant contribution: $D_{UTD}\left(L;\boldsymbol{\rho_d'}-\boldsymbol{R'},-\boldsymbol{\rho_d}+\boldsymbol{R}\right)\sim$

#199158 - $15.00 USD Received 8 Oct 2013; revised 18 Nov 2013; accepted 19 Nov 2013; published 3 Dec 2013

$D_{UTD}\left(L;\boldsymbol{\rho_d'},-\boldsymbol{\rho_d}\right), \forall \boldsymbol{R'},\boldsymbol{R}$, i.e. the "distributed" UTD diffraction coefficient reduces to a constant diffraction coefficient, related to the centers of the regions. Inserting the dominant term in Eq. (21) results in

$$d_{s,l} \sim D_{UTD}\left(L;\boldsymbol{\rho_d'},-\boldsymbol{\rho_d}\right)\delta_{s,0}\delta_{l,0}, \tag{24}$$

where δ is the Kronecker delta symbol. Consequently, the diffracted field in Eq. (19) becomes

$$E_z^{diff}(\boldsymbol{\rho}) \sim -\frac{\omega\mu_0}{4}\sum_{q'=-\infty}^{\infty} a_{q'}H_{q'}^{(2)}(k\rho_d')e^{jq'\phi_o'}D_{UTD}\left(L;\boldsymbol{\rho_d'},-\boldsymbol{\rho_d}\right) \times \frac{1-j}{2}\sqrt{\pi k}\sum_{q=-\infty}^{\infty} J_q(k\rho)H_q^{(2)}(k\rho_d)e^{jq(\phi-\phi_o)}. \tag{25}$$

For a single line source, located at $\boldsymbol{\rho'}$ in the $(\hat{\xi}',\hat{\eta}')$ coordinate system, with unit current density in the $+\hat{z}$-direction and with $\rho' = |\boldsymbol{\rho'}| < R'$, the coefficients $a_{q'}$ are given by

$$a_{q'} = J_{q'}(k\rho')e^{-jq'\phi'}. \tag{26}$$

After substitution of this result into Eq. (25), Graf's addition theorem appears in the first summation. The second summation also corresponds to Graf's addition theorem. The factor in front of this summation hints at the previous use of Eq. (17), which can now be undone. The final result is

$$E_z^{diff}(\boldsymbol{\rho};\boldsymbol{\rho'}) \sim -\frac{\omega\mu_0}{4}H_0^{(2)}(k\,|\,\boldsymbol{\rho_d'}-\boldsymbol{\rho'}\,|)D_{UTD}\left(L;\boldsymbol{\rho_d'},-\boldsymbol{\rho_d}\right)\frac{e^{-jk|-\boldsymbol{\rho_d}+\boldsymbol{\rho}|}}{\sqrt{|-\boldsymbol{\rho_d}+\boldsymbol{\rho}\,|}}. \tag{27}$$

The last expression describes the diffracted field induced by a line source at $\boldsymbol{\rho'}$ in the $(\hat{\xi}',\hat{\eta}')$ system and observed at $\boldsymbol{\rho}$ in the $(\hat{\xi},\hat{\eta})$ system. However, here, the diffraction coefficient is calculated from the centres of the corresponding regions, which is allowed when $\rho_d \gg R$ and $\rho_d' \gg R'$. This result should be compared to Eq. (1), proving the validity of the proposed approach.

3.2. Numerical validation

To assess the accuracy of the formalism, consider the geometry shown in Fig. 3. In this constellation, $\alpha = 30^o$, $\rho_d' = 5\lambda$, $\psi_o' = 45^o$ and $R' = \lambda$ are fixed. The region of interest is moved along a trajectory as shown in the figure (dotted line). The center of the region of interest remains at a constant distance from the edge, $\rho_d = 10\lambda$. The angle ψ_o varies from 15^o to 315^o in steps of 5^o. Also, $R = 2\lambda$. A single line source is placed inside the source region and the field is calculated in a discrete observation point P. The source is placed at $\rho' = 0.8\lambda$ and $\phi' = 0^o$ and is excited with unit current density in the $+\hat{z}$ direction. The observation point P is placed at $\rho = 1.5\lambda$ and $\phi_o = \psi_o - 180^o$. In this way, the field is calculated in a circular arc around the edge.

We choose the above constellation with a discrete line source and discrete observation point to allow a comparison with the exact analytical solution, i.e. the Green's function in the presence of a perfectly conducting wedge [8]. This Green's function is given by

$$G(\boldsymbol{\rho};\boldsymbol{\rho'}) = -\frac{j\pi}{2\pi-\alpha}\sum_{l=1}^{\infty} H_\mu^{(2)}(kr_>)J_\mu(kr_<)\sin(\mu\psi')\sin(\mu\psi), \tag{28}$$

in which $\mu = l\pi/(2\pi-\alpha)$, $r_> = \max(|\,\boldsymbol{\rho_d'}-\boldsymbol{\rho'}\,|,|-\boldsymbol{\rho_d}+\boldsymbol{\rho}\,|)$, $r_< = \min(|\,\boldsymbol{\rho_d'}-\boldsymbol{\rho'}\,|,|-\boldsymbol{\rho_d}+\boldsymbol{\rho}\,|)$ and ψ and ψ' are the angles that $-\boldsymbol{\rho_d}+\boldsymbol{\rho}$ and $-\boldsymbol{\rho_d'}+\boldsymbol{\rho'}$ make with the $\hat{x}$-axis respectively.

#199158 - $15.00 USD Received 8 Oct 2013; revised 18 Nov 2013; accepted 19 Nov 2013; published 3 Dec 2013

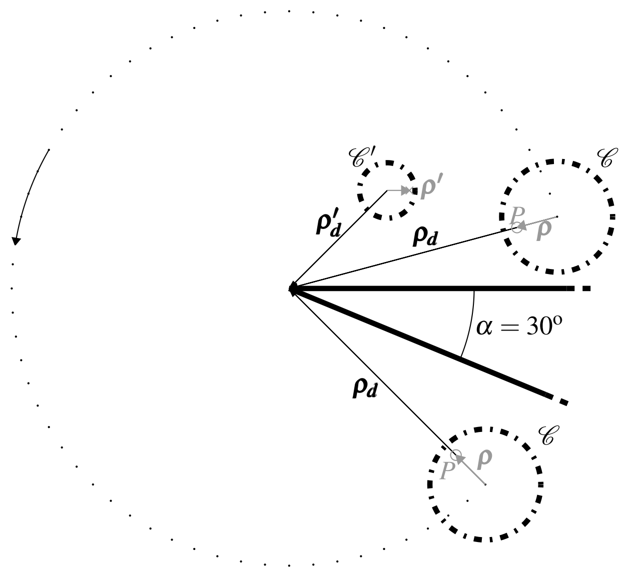

Fig. 3. Configuration for the numerical validation. The region of interest is held at a constant distance from the edge, while changing its angular position. Its trajectory is indicated by means of the dotted line.

The exact result from Eq. (28), when the region of interest moves along the trajectory from $\psi = 15^o$ to 315^o as described above, is presented in the top panel of Fig. 4, together with the results from the new technique. The first result, indicated by crosses (x), is obtained using the traditional diffraction coefficient D_{UTD} in Eq. (21); the second, indicated by circles (o), leverages the improved diffraction coefficient D' of Eq. (23). The error between these two new results and the exact solution is shown in the bottom panel of Fig. 4. An excellent accuracy is observed in regions where the integrand of the 2-D FFT transform of Eq. (21) remains continuous over the integration domain. The integrand is discontinuous for observation angles between 112^o and 158^o (because of the discontinuity of the contribution due to reflection) and also between 202^o and 248^o (because of the discontinuity of the direct contribution). In these regions, the advantage of using the coefficient $D'\left(L;\boldsymbol{\rho}'_d - \boldsymbol{\rho}', -\boldsymbol{\rho}_d + \boldsymbol{\rho}\right)$ is evident. The maximum relative error when adopting $D'\left(L;\boldsymbol{\rho}'_d - \boldsymbol{\rho}', -\boldsymbol{\rho}_d + \boldsymbol{\rho}\right)$ remains bounded to about 1%. This good overall accuracy confirms the validity of the technique outlined in Sec. 2.2.

To obtain these results, the summations over q' and n in Eqs. (19) and (20) were symmetrically truncated to 33 terms, whereas 51 terms were used for the summations over q and m. The series of Eq. (28) was truncated to 203 terms.

4. Application example

To illustrate the full power of the technique, we will now focus on *distributed* sources and regions of interest by investigating the diffraction of a Gaussian beam by a perfectly conducting wedge. During the last few decades, several studies have been devoted to this problem. We refer the reader to [9] for an interesting overview. Most of these approaches are based on the fact that a Gaussian beam is equivalent to a line source in complex space [10] and the diffraction is described based on results for ordinary line sources, e.g. Eq. (28) provides the solution when the wedge is illuminated by a Gaussian beam, provided that $|\boldsymbol{\rho}'_d - \boldsymbol{\rho}'|$ and ψ' are replaced by the complex distance r_b and the complex angle ψ_b given below [9, 11].

The geometry of the problem is illustrated in Fig. 5. A Gaussian beam, originating at

#199158 - $15.00 USD Received 8 Oct 2013; revised 18 Nov 2013; accepted 19 Nov 2013; published 3 Dec 2013

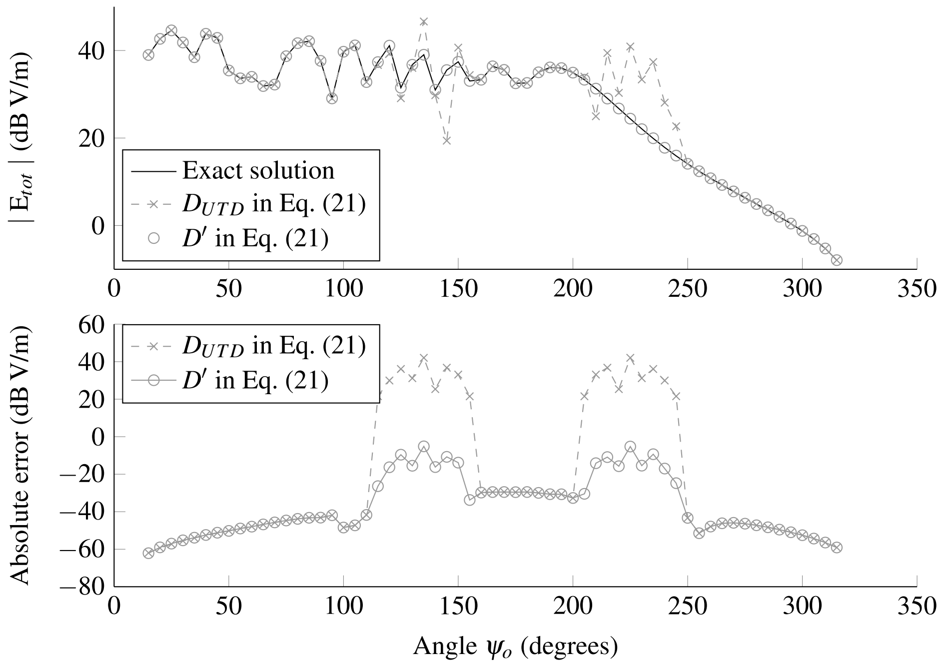

Fig. 4. Top panel: total field at the varying observation point obtained via the exact solution of Eq. (28) (black line) and via the proposed technique of Eq. (19), where the result indicated by crosses (x) is computed relying on the traditional diffraction coefficient, and whereas the result indicated by circles (o) is based on the equivalent UTD coefficient of Eq. (23). Bottom panel: Absolute error. Note that the maximum relative error (not shown in the figure) remains bounded to about 1% when the equivalent UTD coefficient is used.

$\boldsymbol{r_0} = r_0 \cos\psi_0 \hat{x} + r_0 \sin\psi_0 \hat{y}$, with $1/e$-half-width waist $w(\boldsymbol{r_0})$, whose axis in the direction of propagation makes an angle β with the $\hat{x}$-axis, is described in the $(\hat{\xi}', \hat{\eta}')$-system by [10, 11]

$$E_z^{inc}(\boldsymbol{\rho'}) = -\frac{j}{4} H_0^{(2)} \left(k\sqrt{|\, \boldsymbol{\rho_d'} - \boldsymbol{\rho'} \,|^2 + r_b^2 - 2r_b \,|\, \boldsymbol{\rho_d'} - \boldsymbol{\rho'} \,|\, \cos(\psi_b - \psi')} \right), \tag{29}$$

where ψ' is the angle that $-\boldsymbol{\rho_d'} + \boldsymbol{\rho'}$ makes with the $\hat{x}$-axis,

$$r_b = \sqrt{r_0^2 - 2jbr_0 \cos(\beta - \psi_0) - b^2}, \quad \mathscr{R}(r_b) > 0, \tag{30}$$

$$\cos\psi_b = \frac{r_0 \cos\psi_0 - jb\cos\beta}{r_b}, \tag{31}$$

and with $r_0 = 22\lambda$, $\psi_0 = 45^{\text{o}}$, $\beta = 225^{\text{o}}$, $w(\boldsymbol{r_0}) = \lambda/2$ and $b = kw(\boldsymbol{r_0})^2/2$. The wedge has an opening angle $\alpha = 30^{\text{o}}$. A source region defined by the circular contour $\mathscr{C}'$ with center at $\rho_d' = 20\lambda$, $\psi_o' = 45^{\text{o}}$ and radius $R' = 3\lambda$ is positioned around the beam at $\boldsymbol{r_0}$. The coefficients $a_{q'}$ are computed by the substitution of Eq. (29) into Eq. (8). The total field is calculated via Eq. (19) in three completely arbitrarily-shaped regions circumscribed by the following circles:

- $\mathscr{C}_1$: $\psi_{o,1} = 20^{\text{o}}$ and $\boldsymbol{r_0} \cdot \hat{x} = -\boldsymbol{\rho_{d,1}} \cdot \hat{x}$, i.e. the group centre lies beneath the point of origin of the Gaussian beam. Also, $R_1 = 2\lambda$.

- $\mathscr{C}_2$: $\psi_{o,2} = 180^{\text{o}}$, $\rho_{d,2} = 10\lambda$, $R_2 = 3\lambda$.
- $\mathscr{C}_3$: $\psi_{o,3} = 270^{\text{o}}$, $\rho_{d,3} = 15\lambda$, $R_3 = 4\lambda$.

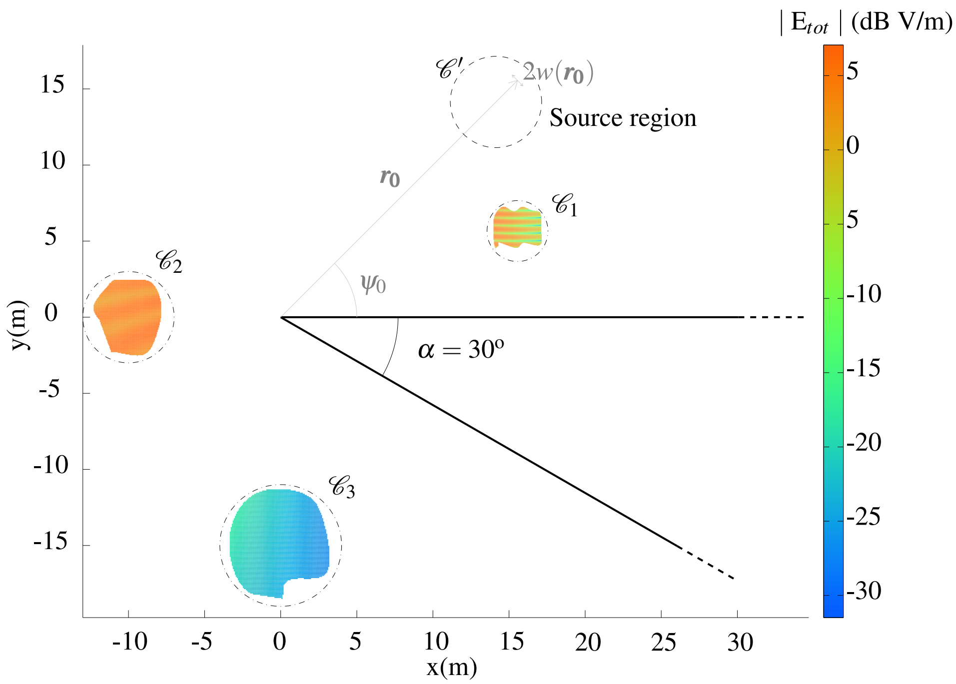

Fig. 5. The total field for an incoming Gaussian beam in the presence of a perfectly conducting wedge.

The results are shown in Fig. 5. In the region of interest enclosed by $\mathscr{C}_1$, a standing wave pattern is observed, which is a consequence of the interference of the incoming beam with its reflection at the upper face of the wedge. The field inside $\mathscr{C}_2$ is mainly dominated by the incoming beam. Some slight variation in the amplitude of the field is visible because of the interference with the diffracted field. The region inside $\mathscr{C}_3$ lies in the shadow of the wedge. Only the diffracted field penetrates this region of space and hence, a low field amplitude is observed.

5. Conclusions

We presented a high-frequency formalism which describes the diffraction of arbitrary incident wavefronts at edges. No matter how complex the light sources may be, it can now be easily dealt with. To start up the simulation, we merely need to know the field emitted by this source over a closed contour. It is proven how the diffracted field in a predefined region of interest can then be expressed in terms of this incident field and a limited set of translation coefficients that take into account the arbitrary nature of the incident wavefront and its diffraction. In the limit of source regions and regions of interest of infinitesimally small dimensions, our solution was shown to reduce to conventional UTD, which confirms the validity of the proposed approach. In the case of a discrete line source, the method proved to be in excellent agreement with the analytic Green's function, especially after the introduction of the novel diffraction coefficient D'.

The advocated formalism considerably increases the range of problems that can be studied using UTD. This was illustrated by investigating the diffraction of a Gaussian beam in Sec. 4, showing that no knowledge about the specific source choice needs to be used explicitly. Moreover, it is important to mention that the proposed technique is easy to implement, as only standard FFT routines are leveraged.

Acknowledgment

The authors would like to thank the Research Foundation Flanders (FWO) for supporting this research.